Science on Natural Resources and Environment
Journal homepage: tapchikhtnmt.hunre.edu.vn

EFFECTS OF MANGROVE DENSITIES AND WIDTH ON WAVE TRANSMISSIONS BY OPEN-SOURCE MODELS

Dao Hoang Tung*, Nguyen Mai Lan
Hanoi University of Natural Resources and Environment, Vietnam

Received 24 October 2023; Accepted 20 December 2023

Abstract

The Mekong deltaic coasts have suffered from erosion and mangrove losses due to many relative threats in human activities, bringing to coastal instabilities. The massive and large number of constructions, such as sea dikes, revetments, and sea walls, tend to break the equilibrium in multiple locations along the coasts. As a result, a significant reduction of mangroves comes along in qualitative and quantitative variations, for example, the number of trees in one location and the healthy width of mangroves. An observation from Google Imagine Engine in multiple sites along the Mekong Deltal coasts shows an average width retreated from 2006 to 2016 was about 60 m. In this study, open-source models, SWAN and SWASH - Developed by Delft University of Technology, are implemented to assess the effect of density and width on wave transmission in Nhat Mat ward, Bac Lieu province, Vietnam. The present results show a significant influence of density on wave transmission, while the larger width of mangroves creates more damping space for waves. Moreover, wave reduction rates (Kt = Ht/Hi, where Hi and Ht are the incoming and transmission wave heights) are related to densities by the power fit. From these results, it is hypothesized that wave height reduction can be predicted via the density of mangroves.

Keywords: SWAN; SWASH; Mangroves; Wave transmission; Mekong delta.

***Corresponding author. Email:** dhtung@hunre.edu.vn

1. Introduction

Mangrove forests are vital to economic development and maintaining the marine ecosystem. Mangroves also bring an equilibrium for the coast between erosion and acceleration with their function. The roots and trunks of mangroves are the keys to wave and flow energy reduction, increasing sedimentation and nutrients for other animals. However, extensive deforestation has been noticed along the Mekong deltaic coast. In particular, the Soc Trang and Bac Lieu provinces' coast has suffered from a massive retreat. A 14-year observation from the Google Earth engine in Figure 1 shows that the mangrove belts are retreated by 40 to 50 m annually. In Figure 1, mangrove edges at the site of Nha Mat ward, Bac Lieu province, in three different years, 2006 (white line), 2016 (green line), and 2020 (blue line), gradually moved landward. The interpretation of mangrove loss might be from the negative feedback of gray-coastal protections [1].

Figure 1: Mangrove belt observation in three different years: 2006, 2016, and 2020

Gray structures always bring safety to coastal areas, especially for essential development sites [1]. However, these structures usually break the balance of sediment transports, including nutrients for mangroves, in which sediments are flushed out at the upstream sites and sunk at the downstream sites. The construction cost for gray structures is also significantly high, but the efficiency is doubly presented. In the past decade, mangroves along the coast of Bac Lieu province, as seen in Figure 1, have been reduced by the presence of sea dike and revetment and climate change [2].

Mangrove forest, on the other hand, is a living system that can adapt to the water level change by retreating landward but keeping its healthy width [3 - 5]. From a coastal engineering perspective, mangroves are the natural defense for the coast, trapping sediments and nutrients [6 - 11]. Many studies about mangroves in the last 10 years have been carried out, giving the inside understanding of wave and flow reduction and studies about nature-based solutions to open a window for coastal protection.

Phan et al., (2014) [12] studied low- and high-frequency attenuation waves inside the mangrove forest using a numerical model, XBeach. The numerical outputs claim a more significant reduction for high-frequency waves than low-frequency ones. This study only presents an efficiency of the mangrove's width on waves without mentioning other contribution parameters, such as the bulk drag coefficients and densities. Kalloe et al., (2022) [13] carried the wave attenuation over vegetation area in a full-scale wave flume in Deltares Academy, the Netherlands. This study points out that the effect of high-density parts of a tree denser than lower tree parts, such as branches, leaves, and body, on wave attenuation is significantly high. Additionally, the experimental results show that one-third of waves tend to be broken at the denser part than the lower part that is usually submerged. Kalloe et al., (2022) also conclude the bulk drag coefficient of the vegetation values at 2 to 3 for the Keulegan - Carpenter number (KC number) of 60 to 80.

Vu Duy Vinh et al., (2010) [14] used the numerical model, Delft 3D - Deltares Academy, to model the wave-vegetation interaction and hydraulic processes in different scenarios in

Bang La, Dai Hop, Hai Phong, Vietnam. The outputs point out the essential roles of vegetation in wave attenuation. This study also claims that wave-induced flow velocities in standard and storm conditions are reduced by 40 to 70 % of incoming waves. Moreover, the role of vegetation is presented in the study of Nguyen Tuan Anh and Nguyen Thi Phuong Thao, (2013), which applies the SWAN model, Delft University of Technology, to simulate wave reduction over the submerged height of a tree.

Furthermore, more independent studies apply open-source, including SWAN (Simulation WAve Near-shore) and especially SWASH (Simulation WAve till SHore), on the interaction between wave and vegetation or other vegetation orientations. Dao et al., (2018) [15] used SWASH to study wave damping due to wooden fences, an array of cylinder media mainly used under the vegetation implementation model. Dao et al., (2021) [16] also validated the SWASH model using a famous bulk drag coefficient - , with laboratory data. More importantly, this drag coefficient is the key for nearly every study for wave-vegetation interactions in the future [17].

Most previous studies only give a few credits for the density, number of cylinders in an area, and the thickness of the location where waves interact to understand the vital key of the bulk drag coefficient in the vegetation. In the Mekong Delta, more than a dozen kinds of mangroves have different characteristics, such as density of body, trunks, and roots, and diameter of body and roots. As mentioned earlier in Figure 1, mangrove widths have significantly decreased by at least 10 m per year from 2006 to 2020. Even though the width retreating and the density reduced by aquaculture activities and breaking equilibrium by gray structures are eventually slowed down by local government and scientists interfering, the functions of mangroves are still worth carrying out. These issues also need to be assessed to compare with the past situations. In this study, the numerical models, SWAN and SWASH, are the primary tools to study wave attenuation over mangrove forests. The outline is the Introduction Method for sections 1 and 2, respectively. Next, the Results and Discussion are in section 3, and the final section is the Conclusion.

2. Numerical models

This study uses numerical models, SWASN and SWASH, to carry out the wave-vegetation interaction. The SWAN is the third generation of real-scale wave simulation in lakes, rivers, seas, and coastal zones. The SWASH model is used for modeling water surface based on non-linear in the shallow areas. Both models are developed and used for most Ph.D. and Post-Doctor research at Delft University of Technology. In the Mekong deltaic coast, it is observed a gentle slope varying from 1:500 to 1:2,000. This particular slope creates a breaking environment for waves during propagation processes, even interacts with the entrance of mangrove forests and creates a highly extended cross-shore profile for the coasts. Phan et al., (2014) [12] also claim that the water depth reaches about 30 m at 100 km offshore. As a result, the computation times become significantly large and waste so many resources. Therefore, the combination of SWAN and SWASH models is considered for wave-vegetation interaction.

2.1. Government equations

The SWAN model applies the wave action balance equation in the shallow water depth, which can be modeled through wave propagation through different topography, reflection, diffraction, and shoaling due to the bottom effect. The government equations are expressed below [18, 19]:

$$\frac{d\vec{x}}{dt} = (c_x, c_y) = \frac{1}{2}\left(1 + \frac{2kd}{\sinh(2kd)}\right)\frac{\sigma\vec{k}}{k^2} + \vec{u} \quad (1)$$

$$\frac{d\sigma}{dt} = c_\sigma = \frac{\partial\sigma}{\partial d}\left(\frac{\partial d}{\partial t} + \vec{u}.\nabla_{\vec{x}}d\right) - \frac{\sigma\vec{u}}{\partial\sigma}c_g\vec{k} \quad (2)$$

$$\frac{d\theta}{dt} = c_\theta = -\frac{1}{k}\left(\frac{\partial\sigma}{\partial d}\frac{\partial d}{\partial m_n} + \vec{k}\frac{\sigma\vec{u}}{\partial m_n}\right) \quad (3)$$

where c_x and c_y are wave orbital velocity in the horizontal and vertical direction, x and y, respectively; c_σ and c_θ are the wave phase velocity in spatial direction, σ and θ, respectively; d is the water depth, k is the wave number, and m_n is the spectral momentum in the n-order.

Next, the SWASH model is the time-domain and multidimensional model for modeling non-hydrostatic and free surface flow based on the non-linear water equations [20, 21]. SWASH model can also model other processes for the low- and high-frequency waves with high accuracy in the shallow zone, such as reflection, diffraction, breaking, and especially vegetation interactions [22 - 25]. The government equations are presented as follows:

$$\frac{\partial u}{\partial x} + \frac{\partial w}{\partial z} = 0 \quad (4)$$

$$\frac{\partial\eta}{\partial t} + \frac{\partial}{\partial x}\int_{-d}^{\eta} u dz = 0 \quad (5)$$

$$\frac{\partial w}{\partial t} + \frac{\partial uw}{\partial x} + \frac{\partial ww}{\partial z} + \frac{1}{\rho}\frac{\partial(P_{nh})}{\partial z} + \frac{\partial\tau_{zz}}{\partial z} + \frac{\partial\tau_{zx}}{\partial x} = 0 \quad (6)$$

$$\frac{\partial u}{\partial t} + \frac{\partial uu}{\partial x} + \frac{\partial wu}{\partial z} + \frac{1}{\rho}\frac{\partial(P_h + P_{nh})}{\partial x} + \frac{\partial\tau_{xz}}{\partial z} + \frac{\partial\tau_{xz}}{\partial x} = 0 \quad (7)$$

where x and z are the horizontal and vertical directions in the Decade coordinate, respectively; u and w are the wave orbital velocities in horizontal and vertical directions, respectively; η is the surface elevation, t is time; the pressure P is separated into non-hydrostatic - P_{nh} and hydrostatic pressures - P_h relative to the water column and water orbital in the water and in the air; the turbulent friction of water is set as default, as well as the bottom friction-c_f that based on the famous Manning coefficient.

The interaction between waves and mangroves is modeled in the vegetation implementation model that uses an array of cylinders in an area as the vegetation. In this model, the characteristics of mangroves include the cylinder diameter, the density - the number of cylinders in an area, and the bulk drag coefficient - $\overline{C_D}$. If the incoming wave height in front of the mangrove belt is H_i, the wave height ($H_{t,x}$) reduction inside the mangrove area can be linearly calculated as:

$$\frac{H_{t,x}}{H_i} = \frac{1}{1 + \tilde{\beta}x} \quad (8)$$

where the parameter $\tilde{\beta}$ is calculated by Suzuki et al., (2019) [25] based on Mendez and Losada (2004) [26]:

$$\tilde{\beta} = \frac{1}{3\sqrt{\pi}}\overline{C_D}DNH_0k\frac{sinh^3(k\alpha H_v) + 3(k\alpha H_v) + cosh^3(k\alpha H_v) - 3(k\alpha H_v) + 2}{[(2kd) + 2kd]sinh(kd)} \quad (9)$$

where the αH_v (m) is the submerged depth of a plant in a vegetation model. Therefore, several parameters can be importantly taken into account, including the vegetation height, density, diameter, and more importantly, the bulk drag coefficient ($\overline{C_d}$).

2.2. Model settings

As mentioned earlier, the average slope of the Mekong deltaic coast is very gentle, including a hill of 1:800 in Bac Lieu province and 1:500 in Ganh Hao province, Vietnam [27]. The maximum tidal height is up to 4.0 m, and the average water level is 1.95 m [28]. As a result, the average tidal flat and mangroves can be developed up to over 1,500 m if the environment is good enough. Additionally, due to a lack of near-shore wave data, simulating offshore waves at a depth of 30 m and the cross-shore distance of 100 km to near-shore is essential in this study.

Since SWAN is suitable for wave energy dissipation from offshore with high-speed computation but less accurate in the shallow zone, SWASH is accurately computed in the shallow water. It consumes incredibly high computer resources and time. Therefore, the combination between two models, SWAN and SWASH, is also essential in this study. Figure 2b introduces the SWAN model boundary with the input boundary on the west side. At the location near-shore, the SWAN output is a set of wave spectrum, insisting significant wave height H_s and peak wave period T_p, is the input for the SWASH model. It is considered as the fast and accurate method for this study. Also, in Figure 2b, the total length of the SWAN model is about 120 km at a depth of 50 m (on the west side), and the output location is 109.5 km on the east side (black dashed line).

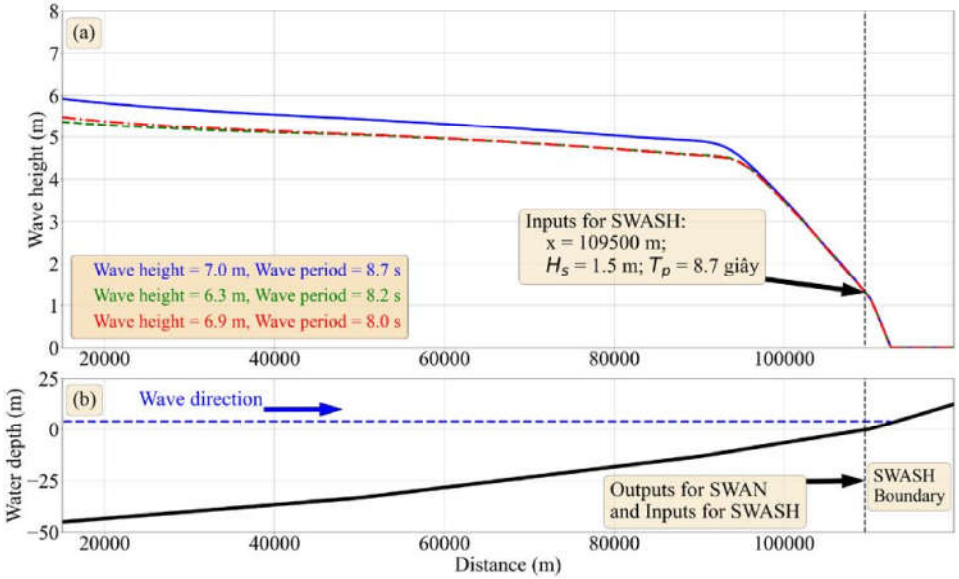

Figure 2: SWAN simulation: (a) Wave height distribution; (b) Model boundary

In Figure 3, the SWASH boundary is set with a total length of 5,000 m at a water depth of 4.0 m, and the slope is set as 1:800, which is observed in Nha Mat, Bac Lieu, Vietnam [27]. The input is again set at the West side, where the wave spectrum, such as H_s and T_p is put.

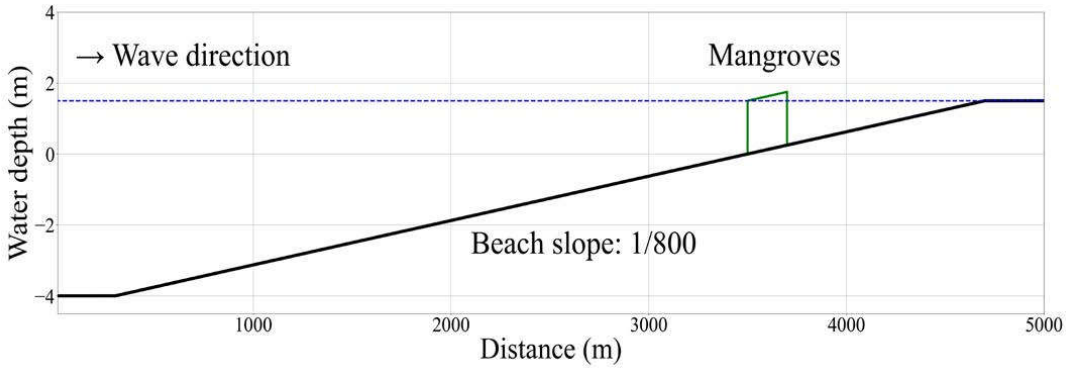

Figure 3: Model boundary for SWASH

Wave characteristics are chosen from an offshore observation at a water depth of 35 m and 100 km landward [29], presented in Table 1. Table 1 shows the statistical waves in maximum values in 12 months. This study chooses wave inputs for the SWAN model (Figure 2, West side) as top waves. In Figure 2a, wave heights along the SWAN boundary for three showcases of January, February, and March show that wave heights are all attenuated to about H_s = 1.5 m at the input location for SWASH at a water depth of 4.0 m.

Table 1. Long-term statistical wave characteristics in Bach Ho Station (1980 - 2010) [29]

Month	I	II	III	IV	V	VI	VII	VIII	IX	X	XI	XII
Maximum (m)	7.0	6.3	6.9	4.5	5.0	4.7	4.0	5.0	5.0	5.0	7.0	10.5
Maximum (s)	8.7	8.2	8.0	10.0	6.8	7.1	7.7	7.0	7.3	8.4	8.4	11.5

Additionally, wave spectral densities for three showcases are presented in Figure 4. Theoretically, waves in the propagation process can be distinguished into several main parts: (1) the peak period with maximum spectral density - this is the period of the wave group, and (2) two smaller peaks for shorter waves. In all showcases shown in Figure 4, wave outputs are shown with peak period with f= 0.6 Hz for the wave group, f = 0.2 Hz, and 0.115 Hz are represented for short waves. Wave-wave interactions can explain the lower frequency. As mentioned, they can all be chosen for SWASH inputs.

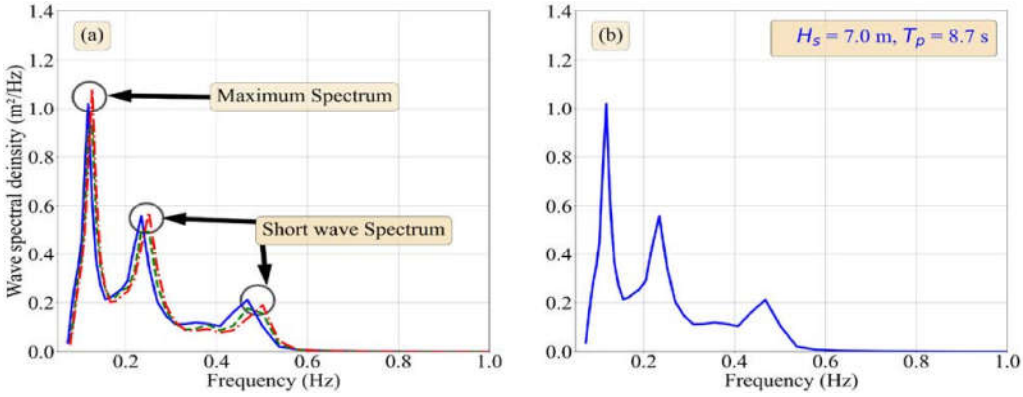

Figure 4: (a) Wave spectral density for three showcases in the SWAN model (x = 109.5 km) and (b) the chosen option for the SWASH model (x = 0 m)

In the SWASH model, several vegetation cases are shown in Table 2 to study wave-vegetation interactions. Their vegetation characteristics are chosen based on previous studies for laboratory [13, 16, 30, 31] and field data [27, 32]. Their vegetation characteristics are chosen based on previous studies for laboratory [13, 16, 30, 31] and field data [27, 32]. Due to it being impossible to mimic different body parts of a mangrove, only the body as a cylinder is used in SWASH. The vegetation height (H_v) and body diameter (D_v) are chosen for only one value of 1.5 m and 0.03 m, respectively. The bulk drag coefficient ($\overline{C}_d$) is based on Dao et al., (2021) for a similar diameter and density as 1.5. Vegetation widths are chosen based on the situation in Figure 1, in which three widths (B_v) varying from 100 to 200 m are claimed. For each width shown in Table 1, vegetation densities (N_v, cylinder. m^{-2}) ranging from 10 to 70 cylinders.m^{-2} are given based on the fact that there are different types of mangroves with other biological characteristics. The observation in the field present in the previous studies, Dao et al., (2018) [15] and Mai et al., (2021) [27], the number of bodies in a square meter reaches a certain number for its maximum. In this study, the healthier width is the largest, and the highest density is the baseline for comparison.

Table 2. Vegetation scenarios for SWASH

Case	Vegetation height (H_v, m)	Diameter (D_v, m)	Width (B_v, m)	Bulk Drag coefficient ($\overline{C}_d$)	Density (N_v, cylinder.)
1	1.5	0.03	200	1.5	10 - 70, N_0 = 70
2	1.5	0.03	150	1.5	10 - 70, N_0 = 70
3	1.5	0.03	100	1.5	10 - 70, N_0 = 70
4	1.5	0.03	50	1.5	10 - 70, N_0 = 70
5	0	0	0	0	0

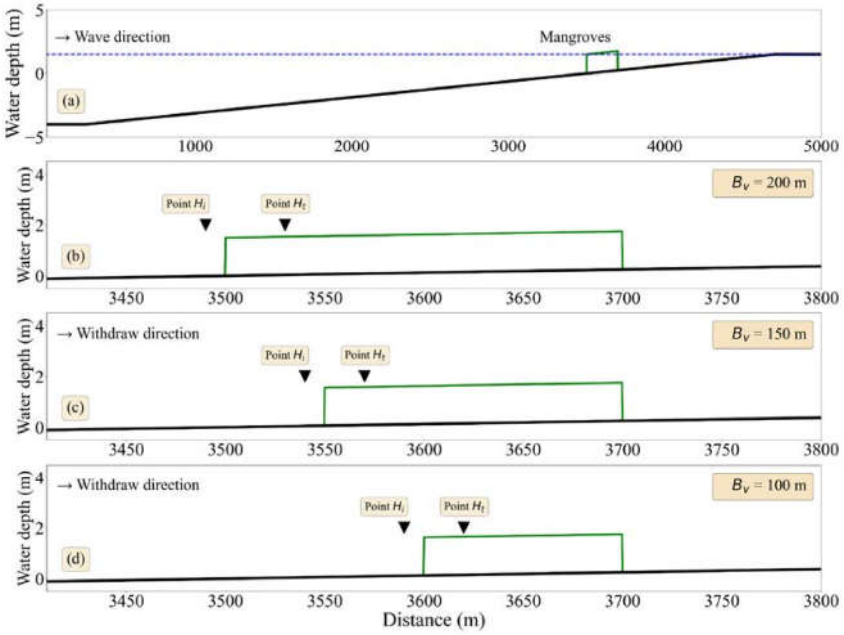

Figure 5: Schematic profile of vegetation in SWASH: (a) Cross-shore profile in SWASH; (b), (c), and (d) are vegetation location and width for each scenario

However, the number of scenarios for simulation in SWASH can be multiplied due to the many densities that need to be tested. At least 31 density tests are carried out, varying from 10 to 70 cylinders.m^{-2}. The total number of tests for all vegetation cases is up to 93 scenarios. Therefore, it is more convenient to test only one wave input, as the spectrum is shown in Figure 4, in which wave height H_s = 1.5 m and T_p = 8.7 s to be specific.

Figure 5 presents the mangrove area that is at x = 3,500 m in the SWASH model. In the vegetation model, mangroves are represented as an array of cylinders, and the arrangement of cylinders is set randomly or inhomogeneous. For each width shown in Figures 5b, 5c, and 5d, mangroves are set to be retreated 50 m following the mentioned theory early in the Introduction section, meaning the retreated direction is the same as the wave direction.

3. Result and discussion

3.1. Wave reduction for different densities

Figure 6 presents wave propagation to the near-shore and mangrove areas (green lines) over the profile. Figure 6b shows wave heights generally keep the same value as 1.5 m until reaching the shallower water depth and breaking at x = 2,000 m. Wave heights are gradually reduced to about 1.0 m at x = 3,500 m before significantly being damped by mangroves. The transmission wave heights behind the mangroves are about 0.1 to 0.2 m.

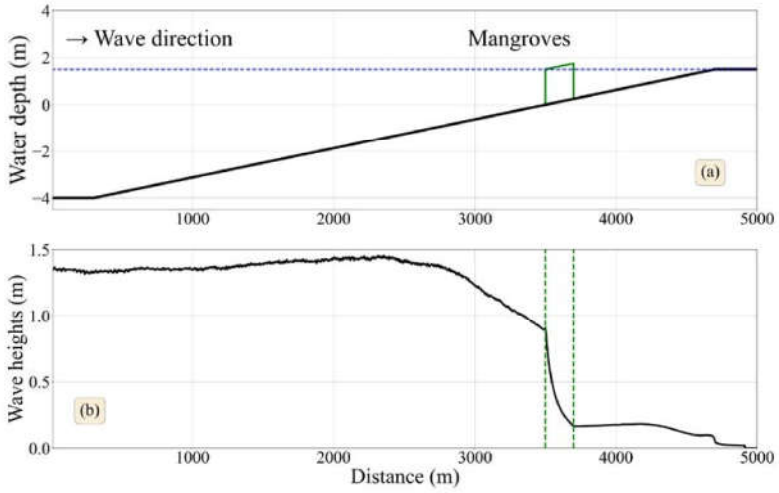

Figure 6: (a) Cross-shore profile and mangrove area; (b) Wave height transformation

In Figure 7, simulated results of wave transforming inside the mangrove widths, B_v = 200 m (Figure 7a), B_v = 150 m (Figure 7b), and B_v = 100 m (Figure 7c), in the different densities ranging from 10 to 50 cylinders.m^{-2}. It is seen that the role of density in wave damping is essential. The less dense of vegetation, the lower wave damping. For all lowest density, 10 cylinders.m^{-2}, wave heights reduce from 0.8 to 0.4 m, but the values are even lower for higher density, greater than 10 cylinders.m^{-2}, such as 30 and 50 cylinders.m^{-2}.

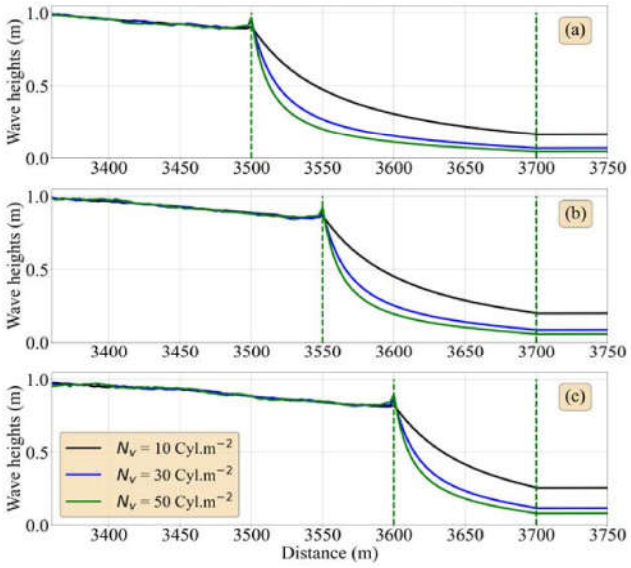

Figure 7: Wave damping over mangrove areas (a) B_v = 200 m, (b) B_v = 150 m, (c) B_v = 100 m

The surface elevations and spectral densities of 4 different vegetation densities at two locations (see Figure 5) in front of the mangrove belt (x = 3,490 m, red lines) and inside the mangrove area (x = 3,520 m, blue lines), are presented in Figure 8. With no mangroves (Figures 8a and 8e), wave energies at the two locations are similar, with a minimal energy loss due to bottom and shallow effects. For the mangrove cases ($N_v > 0$, from Figure 8b to 8h), the larger number of cylinders in an area damps more wave energies, showing that the gap between the upstream point and inside point is narrower with the decrease of density, for example, from N_v = 70 cylinders.m^{-2} (Figure 8b and 8e) to N_v = 25 cylinders.m^{-2} (Figure 8d and 8h).

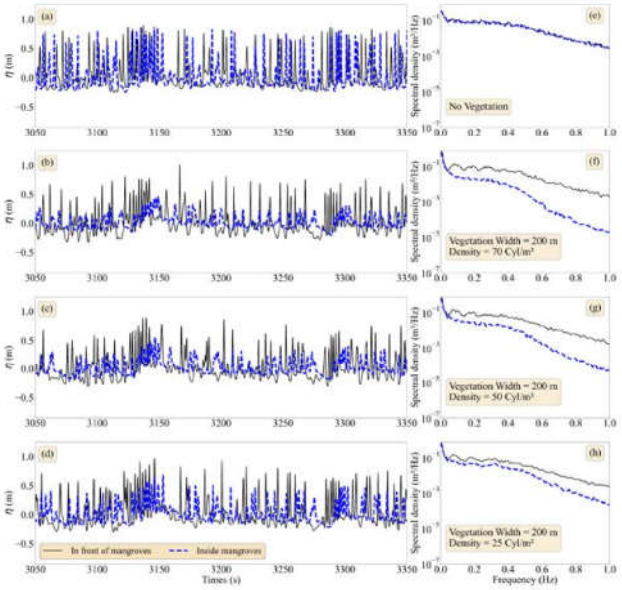

Figure 8: Wave spectrum for different densities (a) N_v = 0; (b) N_v = 70; (c) N_v = 50; (d) N_v = 25 cylinders.m^{-2}

3.2. Wave attenuation in different widths

Figure 9 indicates wave height reduction over mangrove areas in different widths. The role of widths in wave damping efficiency is less significant than the density. Among wave transforming results of different widths, the larger width, B_v = 200 m, the higher wave damping (menegta lines). Over 95 % of incoming wave heights are dissipated inside the mangrove area. Wave heights are reduced less for the most negligible thickness, B_v = 100 m, about 90 % incoming wave energy.

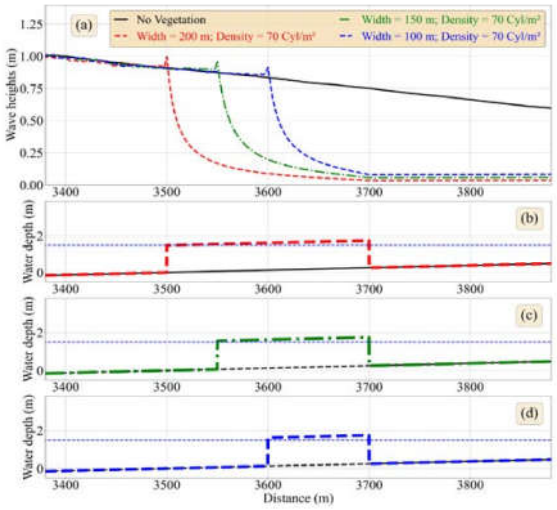

Figure 9: (a) Wave height reduction over different widths of mangroves; (b), (c) and (d) are the schematic mangrove areas in 03 widths: 200 m, 150 m, and 100 m, respectively

However, it should be noted that when waves propagate to the smaller width, they also get damped by bottom and shallow effects, resulting in wave energies before reaching the mangrove belt. In Figure 9a for the case B_v = 100 m (blue dashed lines), wave heights reduce by about 20 % their incoming wave heights at x = 3,400 m before damping to 0.1 m by mangroves.

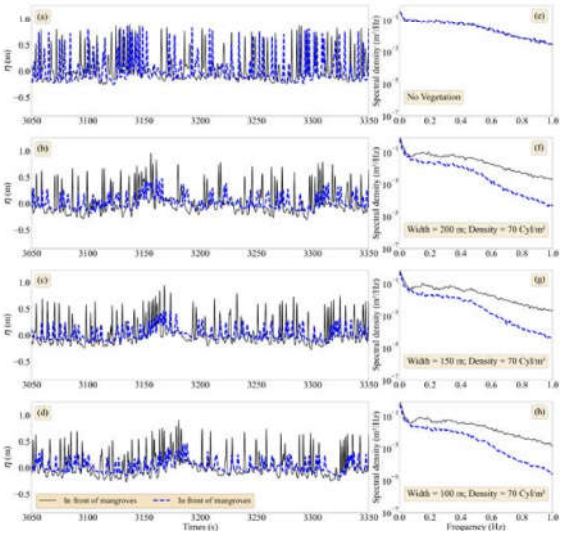

Figure 10: Surface elevation and wave spectral density over different mangrove widths

Figure 10 also presents surface elevation and wave spectrum for different widths, such as B_v = 200 m, 150 m, and 100 m, with the same density of 70 cylinders.m^{-2}. The role of vegetation width, again, is influential when nearly every width damps the same amount of incoming wave energy. Note that the extracted point for incoming is near the mangrove belt (Figure 5). This result also claims that density plays a more significant role than width, even though vegetation width can be the main biological parameter to indicate how healthy mangroves are.

3.3. Relative coefficient for vegetation density and width

Wave transmission coefficient (K_t) is commonly the comparison parameter between incoming and attenuated waves. This coefficient is calculated as:

$$K_t = \frac{H_t}{H_i} \tag{10}$$

where, H_i and H_t are the incoming wave heights and transmitted wave heights inside a mangrove area, respectively. The location for extracting these values is shown in Figure 5.

In Figure 11, transmission coefficients (K_t) are plotted together with the density rate, R_n- N_o/N_v with N_o is the ideal healthy density for mangroves, which is 70 cylinders.m^{-2}. The lower the rate, the higher the simulated density. For example, the value of R_N varies from 1.0 to 3.0, resulting in the density ranges from 20 to 70 cylinders.m^{-2}. From the results in Figure 10, wave energies reduce from 40 % to 60 % of their incomings when R_N ranges from 1.0 to 3.0. Also, the lower wave reduction appears at the higher R_N rate, varying from 4.0 to 5.0.

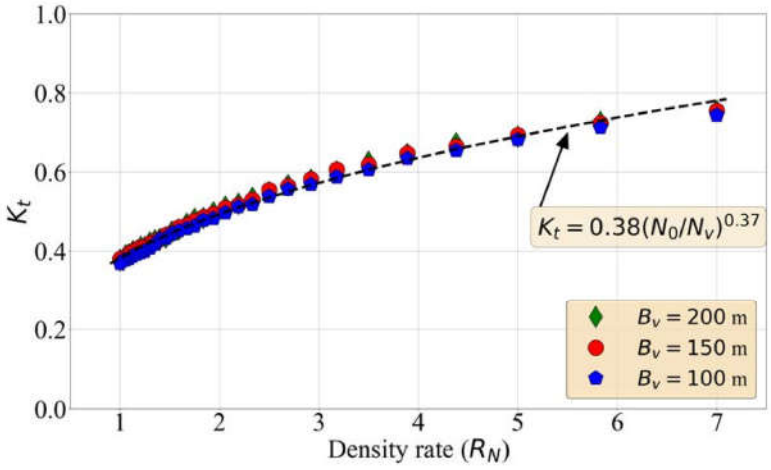

Figure 11: Relationship between transmission coefficient (K_t) and the density ratio (R_N)

Additionally, the relationship between K_t and R_N is concluded within the curve fit, and it can be expressed as

$$K_t = 0.38 \left(\frac{N_0}{N_v}\right)^{0.37} \tag{11}$$

From this equation, it is possible to predict the incoming wave height and design an ideal mangrove forest for future projects via the best option for density.

4. Conclusion

The present study applies the open-source models, SWAN and SWASH, to simulate wave attenuation over an

array of mangrove forest cylinders. The SWAN model is firstly used to simulate wave transformation from offshore to near-shore, and the outputs as the wave spectrum at the near-shore depth are used as inputs for the SWASH model. Both models are previously validated and calibrated, resulting in a certain level of trust for this study. The simulation outputs of the SWASH model indicate the deep information and mechanism of wave-vegetation interaction.

The scenarios for SWASH simulation, including densities and widths, claim that the densities are the key to significantly reducing incoming energies. In contrast, the widths give a lower wave reduction efficiency. However, the widths are indicated as one of the critical parameters for a healthy mangrove forest. The width can be a crucial characteristic of mangroves to reduce the long waves (low-frequency waves). It is shown that the reduction of mangrove width in the past decades resulted in such a disturbing phenomenon: Coastal erosion. Therefore, the result for vegetation width needs to be considered carefully.

Last but not least, the transmission coefficient, K_t, is an excellent parameter to assess the quantity of wave reduction over vegetation. The relationship between K_t and R_N ($R_N = N_o/N_v$) - the density rate is computed as the curve-fit: $K_t = 0.38\ (N_o/N_v)^{0.37}$ opening a new window for future studies of nature-based solutions.

REFERENCES

[1]. T. Schoonees et al., (2019). *Hard structures for coastal protection, towards greener designs*. Estuaries and Coasts, Vol. 42, No. 7, 1709-1729.

[2]. E. L. Gilman, J. Ellison, N. C. Duke, and C. Field (2008). *Threats to mangroves from climate change and adaptation options: A review*. Aquat Bot, Vol. 89, No. 2, 237-250.

[3]. N. C. Duke and K. Schmitt (2015). *Mangroves: Unusual forests at the seas edge, Tropical forestry handbook.* Pancel L., Kohl M.(ed), Springer, p. 24.

[4]. P. N. Hong and H. T. San (1993). *Mangroves of Vietnam*, Vol. 7. IUCN.

[5]. A. E. Lugo and S. C. Snedaker (1974). *The ecology of mangroves*. Annu Rev Ecol Syst, Vol. 5, No. 1, 39-64.

[6]. M. A. Othman (1994). *Value of mangroves in coastal protection*. Hydrobiologia, Vol. 285, No. 1-3, 277-282.

[7]. Y. Mazda, M. Magi, M. Kogo, and P. N. Hong (1997). *Mangroves as a coastal protection from waves in the Tong King delta, Vietnam*. Mangroves and salt marshes, Vol. 1, No. 2, 127-135.

[8]. K. Furukawa and E. Wolanski (1996). *Sedimentation in mangrove forests*. Mangroves and salt marshes, Vol. 1, No. 1, 3-10.

[9]. C. Woodroffe (1992). *Mangrove sediments and geomorphology*. Tropical mangrove ecosystems, 7-41.

[10]. D. Alongi (2009). *The energetics of mangrove forests*. Springer Science & Business Media.

[11]. K. Kathiresan (2003). *How do mangrove forests induce sedimentation?*. Rev Biol Trop, Vol. 51, No. 2, 355-360.

[12]. L. K. Phan, J. S. M. van Thiel de Vries, and M. J. F. Stive (2014). *Coastal Mangrove Squeeze in the Mekong delta*. J Coast Res, 233-243. Doi: 10.2112/JCOASTRES-D-14-00049.1.

[13]. S. A. Kalloe, B. Hofland, J. A. A. Antolínez, and B. K. van Wesenbeeck (2022). *Quantifying Frontal-Surface Area of Woody Vegetation: A Crucial Parameter for Wave Attenuation*. Front Mar Sci, Vol. 9, 820846.

[14]. V. D. Vinh, T. A. Tu, T. D. Thanh, and V. D. Thai (2010). *Hydrodynamics and waves attenuation in the mangrove forest*

in coastal zone of Bang La - Dai Hop (Hai Phong). Conference of Marine Science and Technology, No. V, Vol. 2.

[15]. T. Dao, M. J. F. Stive, B. Hofland, and T. Mai (2018). *Wave Damping due to Wooden Fences along Mangrove Coasts*. J Coast Res, Vol. 34, No. 6, 1317-1327. Doi: 10.2112/JCOASTRES-D-18-00015.1.

[16]. H. T. Dao, B. Hofland, T. Suzuki, M. J. F. Stive, T. Mai, and L. X. Tuan (2021). *Numerical and small-scale physical modelling of wave transmission by wooden fences*.

[17]. T. D. Hoang, L. V. Van, L. N. Thi, and H. V. Thu (2022). *Recovering mangroves with wooden fence along Mekong deltaic coast: physical mechanism and SWASH model*. Journal of Science on Natural Resources and Environment, No. 40, 84-96.

[18]. C. C. Mei (1989). *The applied dynamics of ocean surface waves*. World scientific, Vol. 1.

[19]. G. B. Whitham (2011). *Linear and non-linear waves*. John Wiley & Sons.

[20]. M. Zijlema (2012). *Modelling wave transformation across a fringing reef using SWASH*.

[21]. M. Zijlema, G. Stelling, and P. Smit (2011). *SWASH: An operational public domain code for simulating wave fields and rapidly varied flows in coastal waters*. Coastal Engineering, Vol. 58, No. 10, 992-1012.

[22]. M. Zijlema and G. S. Stelling (2005). *Further experiences with computing non-hydrostatic free-surface flows involving water waves*. Int J Numer Methods Fluids, Vol. 48, No. 2, 169-197.

[23]. P. Smit, M. Zijlema, and G. Stelling (2013). *Depth-induced wave breaking in a non-hydrostatic, near-shore wave model*. Coastal Engineering, Vol. 76, 1-16.

[24]. D. P. Rijnsdorp, P. B. Smit, and M. Zijlema (2012). *Non-hydrostatic modelling of infragravity waves using SWASH*. Coastal Engineering Proceedings, Vol. 1, No. 33, p. 27.

[25]. T. Suzuki, Z. Hu, K. Kumada, L. K. Phan, and M. Zijlema (2019). *Non-hydrostatic modeling of drag, inertia and porous effects in wave propagation over dense vegetation fields*. Coastal Engineering.

[26]. F. J. Mendez and I. J. Losada (2004). *An empirical model to estimate the propagation of random breaking and nonbreaking waves over vegetation fields*. Coastal Engineering, Vol. 51, No. 2, 103-118.

[27]. C. Mai Van, A. Ngo, T. Mai, and H. T. Dao (2021). *Bamboo fences as a nature-based measure for coastal wetland protection in Vietnam*. Front Mar Sci, Vol. 8, p. 1430, [Online]. Available: https://www.frontiersin.org/article/10.3389/fmars.2021.756597.

[28]. S. Tas (2016). *Coastal protection in the Mekong Delta: Wave load and overtopping of sea dikes as function of their location in the cross-section, for different foreshore geometries*.

[29]. V. H. Hoang and H. N. Nguyen (2006). *Result on study of wave field on Dong Nai, Sai Gon estuaries and suggestion of sea bank and river mouth protection methods*. Vietnam-Japan Estuary Workshop in collaboration between Tohoku University and Water Resources University, 140-150.

[30]. K. L. Phan, M. J. F. Stive, M. Zijlema, H. S. Truong, and S. G. J. Aarninkhof (2019). *The effects of wave non-linearity on wave attenuation by vegetation*. Coastal Engineering, Vol. 147, 63-74.

[31]. T. Mai, T. Dao, A. Ngo, and C. Mai (2019). *Porosity Effects on wave transmission through a bamboo fence*. International Conference on Asian and Pacific Coasts, 1413-1418.

[32]. H. T. Dao, B. Hofland, M. J. F. Stive, T. Mai, and A. Ngo (2022). *Design considerations for brushwood fences concerning bathymetry and fence locations*. Proceedings of the 2nd Vietnam Symposium on Advances in Offshore Engineering: Sustainable Energy and Marine Planning, 238-245.